A year-long observational analysis of atmospheric trace gases and particulate matter in Kathmandu

Dikra Prasad Bajgai, Sagar Adhikari, Arshini Saikia, Bertrand Bessagnet, Suresh Pokhrel, Govinda Lavincchane, Deepak Gyawali, Ravi Sahu, Qianggong Zhang

A year-long observational analysis of atmospheric trace gases and particulate matter in Kathmandu.

Dikra Prasad Bajgai[a,1,*], Sagar Adhikari[a], Arshini Saikia[a], Bertrand Bessagnet[a,c], Suresh Pokhrel[a], Govinda Lamichhane[b], Deepak Gyawali[b], Ravi Sahu[a], Qianggong Zhang[a]

[a] *International Centre for Integrated Mountain Development (ICIMOD), G.P.O. Box 3226, Kathmandu, Nepal*
[b] *Ministry of Forests and Environment, Department of Environment, Babarmahal, Kathmandu, Nepal*
[c] *LMD/IPSL, École Polytechnique, Institut Polytechnique de Paris, ENS, PSL Research University, Sorbonne Université, CNRS, Palaiseau, France*

Abstract

Kathmandu Valley is one of the most densely populated cities in Nepal, facing significant air quality challenges. This study presents a comprehensive analysis based on twelve months of continuous air quality measurement data collected at the Khumaltar Air Quality Monitoring Station (ICIMOD AQMS), which is located in the southern part of the Kathmandu Valley. The study investigates particulate matter (PM_{10}, $PM_{2.5}$, PM_C (PM_{10} - $PM_{2.5}$)) alongside trace gases (O_3, NO_x, SO_2, and CO), focuses on their seasonal, diurnal variations, interspecies correlations, potential sources, and the impact of regional atmospheric transport. The results reveal that the annual $PM_{2.5}$ concentration (49 $\mu g\ m^{-3}$) largely exceeds the WHO air quality guideline of 5 $\mu g\ m^{-3}$. Pollutant concentrations show clear seasonal variation, with peaks during the winter and pre-monsoon seasons, and a noticeable decline during the monsoon. A strong correlation ($r = 0.82$, $p = 0.00$) between $PM_{2.5}$ and NO_x indicates that fossil fuel combustion is a dominant source of fine particulate pollution. During the pre-monsoon season, O_3 concentrations

*Corresponding author at: International Centre for Integrated Mountain Development (ICIMOD), Khumaltar, Lalitpur, Nepal.

Email address: dikrapb@gmail.com (Dikra Prasad Bajgai)

[1] Current address: Forschungszentrum Jülich GmbH, Institute of Climate and Energy Systems, Jülich, Germany

occasionally exceed 100 ppb (8-hr running average), with seasonal diurnal concentration observed close to 90 ppb in the afternoon. The study found that temperature and relative humidity significantly influence coarse PM levels, with a strong negative correlation (r = -0.89, p = 0.00) between coarse PM and the relative humidity, suggesting less resuspension under moist conditions. Furthermore, this study highlights the severe air pollution in the Kathmandu Valley throughout the year, driven primarily by local emissions, with regional atmospheric transport further contributing to poor air quality.

Keywords: Air quality monitoring, Trace gases, Interspecies correlation analysis, Regional atmospheric transport, Coarse particulate matter

1. Introduction

Rapid urbanization, industrialization, and economic growth contribute to air pollution through the emission of reactive gases and particulate matter (PM) into the atmosphere (Huszar et al., 2022; Wang et al., 2019). PM and gaseous pollutants such as nitrogen oxides (NO_x), carbon monoxide (CO), sulfur dioxide (SO_2), and ground-level ozone (O_3) are the main pollutants that affect air quality. These pollutants are derived from natural and anthropogenic sources, such as combustion of fossil fuels in industries and energy sectors, waste burning and disposal emissions (Liao et al., 2017; Qin et al., 2006; Dentener et al., 2005), and road traffic emissions (Colvile et al., 2001; Castells-Quintana et al., 2021). However, O_3 is produced as a secondary pollutant through the complex photochemical process involving volatile organic compounds (VOC), CO, and NO_x interacting with solar radiation. The key mechanism involves radical-driven oxidation cycles (e.g., HO_X chemistry) that promotes NO_2 reformation and amplify O_3 formation, which depends non-linearly on the VOC/NO_x ratio (Sun et al., 2010; Collins et al., 2002; Crutzen, 1973). These air pollutants are responsible for severe risk to human health (Nuvolone et al., 2018; Liu et al., 2013), crop production, and climate change (Bender and Weigel, 2009). A study also found that air pollution accelerates the corrosion and soiling of building materials, with the extent of damage influenced by local pollutant concentrations (Tzanis et al., 2011).

A recent study revealed that exposure to air pollution was responsible for 8.1 million premature deaths globally in 2021, making it the second-leading environmental risk factor for global mortality after high blood pressure. The report also indicates that air pollution contributes significantly to mortality,

accounting for approximately 30% of deaths from lower respiratory infections, 28% from ischemic heart disease, and 48% from chronic obstructive pulmonary disease (State of Global Air, 2024). In addition, air pollution issues remain significant throughout the world and especially in South Asia (Brunekreef, 2010). A recent study by World Bank (2025) estimated that air pollution contributes to approximately 26,000 premature deaths annually in Nepal, shortening the average life expectancy by about 3.4 years. Mainly, the study found that the air pollution in Nepal is linked to a significant share of disease burden, contributing to 75% of COPD (chronic obstructive pulmonary disease) cases, 46% of strokes, 44% of ischemic heart disease, 41% of lower respiratory infections, 38% of lung cancer, 30% of neonatal complications, and 20% of diabetes cases.

Several studies show that air pollution is alarming in the Hindu Kush Himalayan (HKH) region, including the Kathmandu Valley (Dhital, 2024; Wester et al., 2019; Panday and Prinn, 2009). Kathmandu Valley is the largest and rapidly urbanized city in Nepal, facing serious air quality issues. A study found that the major sources of air pollution in the Kathmandu Valley are dominated by the transport sector, which accounts for 30%–55% of total emissions. This is followed by the commercial sector (10%–35%) and industrial activities (7%–17%) (Sadavarte et al., 2019). Some other studies have also identified that the primary sources of air pollution in the Kathmandu Valley are vehicular emissions (Das et al., 2022; Faiz et al., 2006), industries (Zhong et al., 2019), open waste burning (Das et al., 2018), long-distance transport (Bhardwaj et al., 2018), aircraft emissions (Bajgai and Shrestha, 2023), and construction activities. In addition, vehicular and industrial pollution contribute significantly to the levels of NO_x, CO, VOCs, and PM in the atmosphere (González et al., 2017; Zhong et al., 2019). For SO_2, the brick industries and vehicular emissions contribute significantly to air pollution in the Kathmandu Valley (Zhong et al., 2019).

Poor air quality in urban areas is largely attributed to rapid population growth, industrial expansion, heavy traffic, and poorly maintained road infrastructure, compounded by the slow adoption of cleaner technologies (Castells-Quintana et al., 2021). In addition to anthropogenic emissions, urban air pollution is also influenced by local and regional meteorological factors, which play an important role in the transformation, dispersion, and removal of pollutants from the atmosphere (Zhang et al., 2018b). Few studies have reported the characteristics of pollutants and their relationship with meteorological factors in Kathmandu valley (Bhardwaj et al., 2018; Mues et al.,

2017; Pudasainee et al., 2006), but these are limited to a few pollutants and specific seasons only. However, the relationship between PM, its coarse fraction, and its correlation with meteorological conditions remains unclear. PM is commonly classified based on particle size, such as PM_{10} (particles with an aerodynamic diameter ≤ 10 μm), and $PM_{2.5}$ (particles with an aerodynamic diameter ≤ 2.5 μm), the so called fine particulate matter. The coarse fraction (PM_C) refers to particles with aerodynamic diameters between 2.5 μm and 10 μm, representing the size range between $PM_{2.5}$ and PM_{10}. These particles have their own impact on human health and the climate. $PM_{2.5}$ is strongly associated with health risks due to its ability to penetrate deeply into the lungs and bloodstream, while PM_C is linked to environmental impacts, including reduced visibility and surface deposition (Maciejewska, 2020; Mukherjee and Agrawal, 2017). Study found that the toxic metals are present in PM, including within its nanoparticle fraction, highlighting the potential health risks associated with exposure to these pollutants (Islam et al., 2022; Phairuang et al., 2021). The PM_C study is important because it originates mainly from non-combustion sources such as road dust, construction, and resuspension.

However, PM_C research in the Kathmandu Valley remains extremely limited. Studies from regions with urban characteristics, such as Delhi, offer valuable insights. For instance, near-road particle suspension due to flow is known to contribute to a large amount of total PM_C, often exceeding 20 – 30% (Matthaios et al., 2022). Particle resuspension in Delhi was found to contribute up to 79% of traffic-related PM emissions (Singh et al., 2020), highlighting the significance of non-exhaust sources. This is especially relevant for Kathmandu, where rapid urbanization, unpaved roads, and high traffic density (Khanal et al., 2017). Moreover, as vehicle fleets modernize and exhaust emissions decline, the relative contribution of non-exhaust PM sources is expected to increase (Wang et al., 2022). European studies also emphasize the growing importance of resuspended road dust in urban PM_C levels, which can inform future mitigation strategies. In a local context, Gautam et al. (2005) conducted a study on the impact of accumulated road dust, particularly on roads adjacent to vegetation, on heavy metal concentrations in Kathmandu.

Moreover, recent year-long studies in the Kathmandu Valley are limited, primarily due to the lack of continuous, long-term ground-level measurement data. Most existing research has been based on campaign-based monitoring projects (e.g., SusKat - Sustainable Atmosphere for the Kathmandu Valley

Bhardwaj et al. (2018)) conducted through specific projects. Additionally, model-based research is insufficient to capture seasonal variation in Kathmandu Valley (Adhikary et al., 2007). To understand spatio-temporal variation in response to the source and characteristics of pollutants, this study focuses on characterizing atmospheric trace gases (O_3, NO_x, CO, and SO_2) and particulate matter (PM_{10}, PM_C and $PM_{2.5}$) within the Kathmandu Valley. For this study, we used data from the International Centre for Integrated Mountain Development (ICIMOD) Air Quality Measurement Station (Khumaltar AQMS), located in the Khumaltar subdistrict of the Lalitpur district (south of Kathmandu Valley), during a full annual cycle from 1^{st} October 2022 to 30^{th} September 2023. This study presents the findings from a year-long analysis of trace gases and particulate matter at the Khumaltar AQMS, including seasonal characteristics, interspecies correlation, regional transport influences, and the relationship between coarse PM and local meteorological parameters.

2. Materials and Methods

2.1. Site description

The Khumaltar AQMS (27^o $38'$ $45.55''$N; 85^o $19'$ $25.71''$E, Elevation: 1325m a.s.l.) is located in Khumaltar in the southern part of the Kathmandu valley, 6 km away from the city center (Figure 1). Khumaltar is characterized by a mix of urban buildings, residential houses, and some government offices, interspersed with agricultural land. The AQMS is situated on the top floor of a three-story building, approximately 20 m above ground level. This station serves as a permanent air quality measurement site and a demonstration center for ICIMOD. It is equipped with instruments for monitoring meteorological parameters and atmospheric composition.

2.2. Measurements description

Particulate matter and atmospheric trace gases were continuously monitored at Khumaltar AQMS, and the data were considered from October 2022 to September 2023 using state-of-the-art instruments described subsequently. PM_{10} and $PM_{2.5}$ were monitored with a Grimm EDM-180 (Aerosols Technik, Germany). The instrument operates on the principle of single-particle light scattering: as particles pass through a focused 660 nm diode laser beam, the scattered light intensity is detected and used to determine particle size and

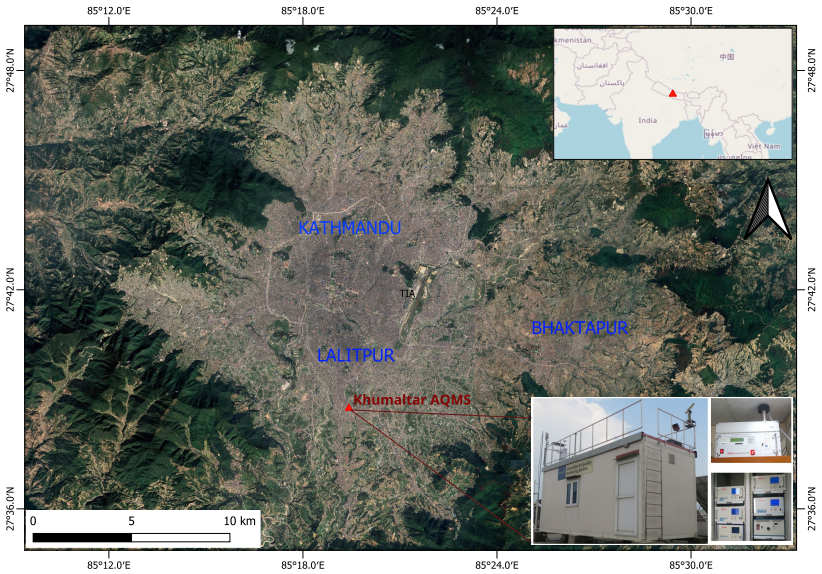

Figure 1: Location of the Khumaltar/ICIMOD Air quality monitoring station.

number concentration across 31 channels. The mass concentration of particulate matter was derived from the measured size distributions using built-in manufacturer algorithms (Grimm and Eatough, 2009). The instrument operated at a sample airflow rate of 1.2 liters per minute (LPM). The typical measurement uncertainty is ± 3 % for particle number concentration and ± 5 % for mass concentration, as specified by the manufacturer's calibration and supported by field validation.

O_3 was measured using an ultraviolet (UV) photometric ozone analyzer (Model 49i, Thermo Scientific, USA) with a minimum detection limit of 1 ppb and a measurement uncertainty of typically ± 1-2%. The ozone analyzer operates on the principle that O_3 molecules absorb UV radiation at a wavelength of 254 nm, as described by the Beer-Lambert law. The intake ambient air sample flows through a teflon tube at a rate of 1 LPM. CO concentrations were continuously measured using a CO analyzer (Model 48i, Thermo Scientific, USA), which operates on the principle of infrared radiation absorption at a wavelength of 4.6 microns by CO molecules. The analyzer has a minimum detection limit of 0.04 ppm and a precision of ± 1 % ppm. The air intake flow rate of the CO analyzer was 1 LPM. NO_x (NO, NO_2) measurements were measured using the Model 42i analyzer (Thermo

Scientific, USA). The analyzer uses the principle of chemiluminescence to measure NO-NO_2-NO_x concentrations in the air, where NO reacts with O_3 to produce light proportional to NO concentration. For NO_2 measurement, NO_2 is converted to NO using a heat molybdenum converter (approximately 325 °C temperature), and the total NO_x is determined accordingly, with a minimum detection limit of 0.4 ppb (1-minute averaging) and the precision ± 0.4 % and the sample inlet flow rate 0.6 LPM. SO_2 was measured using a Model 43i (Thermo Scientific, USA) instrument, which is based on the principle that SO_2 molecules absorb ultraviolet (UV) light at a specific wavelength to transition into an excited state and then decay back, emitting UV radiation at different wavelengths. The detection limit of the analyzer is 0.5 ppb, and the measurement range is 0–50 ppb with a precision of ± 1 % of the reading. The air intake flow rate of the analyzer was 0.5 LPM.

In addition, the Thermo Scientific Dynamic Gas Calibrator (Model 146i) and the Zero Air Supply (Model 1160) with certified calibration gas mixture were used for multipoint calibrations of NO_x, CO, and SO_2 analyzers. The O_3 analyzer was calibrated using activated charcoal for zero calibration and an internal O_3 generator for span calibration. The meteorological parameters, including temperature, relative humidity, wind speed, rainfall, and atmospheric pressure, were measured using a Compact Weather Sensor (Lufft, Germany) during the study period. Quality assurance procedures, including calibration, maintenance, and other events, were meticulously recorded in the station maintenance logbook, and the information was used during the data analysis. Eventually, only validated data were considered for analysis, while measurements affected by calibrations, routine maintenance, power failures, or instrument noise were excluded during the initial data cleaning stage. Overall, the measurement data show excellent completeness, with valid data coverage for more than 95 % days for PM (PM_{10} and $PM_{2.5}$) and approximately 90 % days for O_3, NO_x, CO, and SO_2. All the instruments were under the routine maintenance and calibration procedures as prescribed by the manufacturer. The list of instruments and brief information is summarized in Table 1.

2.3. Statistical analysis

The analysis was conducted using open-source Python libraries (Python scripting). Pearson correlation coefficients (r) along with their corresponding p-values were calculated to assess the strength and statistical significance of

Table 1: Details of the instruments used in this study in the Khumaltar AQMS with a one-minute temporal resolution.

Name of Instrument (Model)	Manufacturers	Parameters/Pollutants
Environmental dust monitor (EDM 180)	Grimm Aerosol Technik, Germany	PM ($PM_{2.5}$, PM_{10})
O_3 Analyzer (Model 49i)	Thermo Scientific, USA	O_3
CO Analyzer (Model 48i)	Thermo Scientific, USA	CO
NO_x Analyzer (Model 42i)	Thermo Scientific, USA	NO_x (NO_2 and NO)
SO_2 Analyzer (Model 43i)	Thermo Scientific, USA	SO_2
Smart Weather Sensor (WS700-UMB)	G. Lufft Mess- und Regeltechnik GmbH, Germany	T, RH, RF, WS, WD, P †
Biral visibility sensors (SWS-100LW)	Bristol Industrial and Research Associates, UK	Visibility

† Note: T- temperature, RH – relative humidity, WS- wind speed, WD- wind direction, RF- rainfall, P- Pressure.

the relationships between pollutants and meteorology. The specific correlations analyzed included the relationship between NO_x and O_3, NO_x and SO_2, O_3 and $PM_{2.5}$, NO_x and $PM_{2.5}$. Additionally, the relationship between PM coarse fraction percentage (PM_{cf}), coarse PM (PM_C), and meteorology was examined. The following formulas (1) and (2) were used to calculate the PM_C and PM_{cf} percentage, respectively.

$$PM_C = PM_{10} - PM_{2.5} \tag{1}$$

Where PM_C is the coarse fraction of particulate matter at a given time.

$$PM_{cf}(\%) = \frac{PM_{10} - PM_{2.5}}{PM_{10}} \times 100 \tag{2}$$

Where, PM_{cf} is the coarse fraction of particulate matter at a given time, PM_{10} is the concentration of particulate matter with an aerodynamic diameter equal to or less than 10 micrometers, and $PM_{2.5}$ is the concentration of particulate matter with an aerodynamic diameter equal to or less than 2.5 micrometers.

2.4. Air mass back trajectory cluster

The seasonal air mass back trajectories for the Khumaltar AQMS station were calculated using the National Oceanic and Atmospheric Administration (NOAA) Air Resources Laboratory's Hybrid Single-Particle Lagrangian Integrated Trajectory (HYSPLIT) model. The cluster analysis of the HYSPLIT model reduces spatial variability among trajectories by grouping them into a specified number of clusters (Stein et al., 2015). The number of clusters was determined based on the inflection point in total spatial variance (TSV) reduction and visual inspection of cluster separation (Yu et al., 2025).

These trajectories were clustered using HYSPLIT's built-in clustering algorithm, which minimizes TSV across trajectory endpoints (Cui et al., 2021). To calculate the trajectory, the method used in the trajectory model runs a frequency analysis on the Linux-based HYSPLIT v5 with the $1^\circ \times 1^\circ$ grid with a temporal resolution of 6 hours and the final meteorological database from the Global Data Assimilation System (GDAS) wind field reanalysis data (available at ftp://arlftp.arlhq.noaa.gov). The GDAS dataset is organized weekly with complete records, providing key meteorological variables such as wind components, temperature, and humidity. In this research, the backward trajectories were computed at 100 m above ground level from the Khumaltar AQMS. This elevation was chosen to represent near-surface atmospheric transport and falls within the planetary boundary layer (PBL) height of the Kathmandu Valley. Mues et al. (2017) revealed that the planetary boundary layer (PBL) height in the Kathmandu Valley typically ranges from 150 m to 1460 m throughout the year, varying with time of day, night, and seasonal conditions.

2.5. Meteorological analysis

Table 2 shows the average monthly meteorological parameters at the Khumaltar AQMS station, such as temperature, RH, rainfall, wind speed, pressure, and visibility. This suggests evident attributes of air temperature in winter and monsoon in Kathmandu Valley. Additional data from Tribhuvan International Airport, Kathmandu (VNKT), were downloaded from the University of Wyoming surface data portal (https://weather.uwyo.edu/surface/). As expected, the mean wind speed recorded at the Khumaltar AQMS station is lower compared to that of Kathmandu Airport due to the obstacles and buildings surrounding the stations.

The monthly average temperature was from 10°C in January to 24°C in June. In August, there was a higher relative humidity along with a substantial total rainfall of 216 mm. Similarly, June and July experienced comparable rainfall amounts, approximately 207 mm, while the winter season saw little to no rainfall. Rainfall is rare in winter, leading to low dispersion conditions suggested by the lowest recorded wind speeds and the highest atmospheric pressures. The better visibility conditions occur from July to October, a period during which other meteorological factors also contribute to keeping the valley cleaner.

In this study, seasonal classification was based on climatological criteria that are widely used in Nepal. Specifically, pre-monsoon (March-May) is

Table 2: General meteorological parameters with standard deviations at ICIMOD station and Kathmandu Tribhuvan International airport (only for wind speed) from October 2022 to September 2023.

Month, Year	Temperature (°C)	Relative Humidity (%)	Rainfall (mm)	Wind Speed ICIMOD (m/s)	Wind Speed Airport (m/s)	Pressure (hPa)	Visibility (km)
October, 2022	19.2±1.8	76.7±9.3	-	1.3	3.8	868.1	29.6
November	15.2±1.2	74.7±3.1	-	1.0	3.5	868.8	14.9
December	11.8±1.3	74.5±3.1	-	1.0	3.1	867.7	12.2
January, 2023	10.8±1.6	66.2±8.0	0.0	1.1	3.1	868.9	10.0
February	14.0±1.4	65.4±5.8	11.5	1.5	3.2	867.3	9.6
March	16.1±1.2	63.9±9.5	87.9	1.5	3.4	867.3	12.5
April	19.4±2.8	53.2±13.6	55.5	1.4	3.4	865.4	12.4
May	20.7±2.3	65.5±14.3	144.4	1.5	3.5	864.5	17.4
June	24.4±1.0	69.6±13.8	207.4	1.9	3.7	860.8	26.2
July	23.7±0.8	87.2±3.5	207.6	1.8	3.3	861.9	35.1
August	23.4±1.1	89.2±5.3	216.8	1.7	3.3	861.0	32.6
September	23.7±1.0	81.7±3.9	80.9	1.7	3.6	864.0	38.3

marked by rising temperatures and increased convective activity, and during the monsoon season (June-September), Nepal receives approximately 80% of the annual precipitation (Karki et al., 2016). The post-monsoon season (October-November) is transitional, with decreasing precipitation and cooler temperatures, while the winter season (December-February) is often dry and cold, especially in higher elevations (Karki et al., 2017). This seasonal delineation is commonly used in climatological studies and reflects the temporal distribution of precipitation and temperature patterns across Nepal(Bagale, 2024; Maharjan et al., 2023)

3. Result and Discussion

3.1. Concentration level of air pollutants

The daily concentration (average 24 h) of PM and gaseous pollutants observed at Khumaltar AQMS is illustrated in Figure 2 for the study period. It shows a significant variation in all pollutants over the 12 months (October to September). To evaluate the overall level of pollution concentration compared to the World Health Organization (WHO) air quality guidelines (WHO, 2021) and the National Ambient Air Quality Standard for Nepal (NAAQS, 2012). Figure 2 shows the time series of PM_{10}, $PM_{2.5}$, PM_C, O_3, CO, NO_x, and SO_2 concentrations over the measurement period. The results indicate that the fine particulate matter exceeded the daily WHO air quality guideline of 15 $\mu g\ m^{-3}$ throughout most of the days in a year, except for 81 days during the monsoon and post-monsoon seasons. Furthermore, $PM_{2.5}$ levels exceeded the NAAQS limit of 40 $\mu g\ m^{-3}$ on more than two hundred

days in a year. The annual average concentration (± standard deviation) of $PM_{2.5}$ is 49 ± 26 $\mu g\ m^{-3}$ which is more than nine times higher than the WHO annual limit (5 $\mu g\ m^{-3}$).

The time series shows that the daily PM_{10} concentration ranges from 7 $\mu g\ m^{-3}$ to 245 $\mu g\ m^{-3}$during the study period. With the annual average concentration of PM_{10} is 91 ± 48 $\mu g\ m^{-3}$. The lowest concentrations (below 12 $\mu g\ m^{-3}$) occur two days in June, seven days in August, and three days in September and October. During this period, there was continuous rain with intensity ranging from 0.5 mm/hr to 12 mm/hr. Due to this persistent rainfall, particles might be removed from the atmosphere and deposited onto Earth's surfaces, such as soil, vegetation, and urban infrastructure, through wet deposition processes. Overall, the lowest concentration of particulate matter was found during the rainy days, and the concentration of PM, including coarse particles, was higher during the dry period. The result shows that the daily concentration of PM_C increases consistently from October to the end of March, with significant variations from April to the end of June. This variation is linked to the level of rainfall intensity and duration. During rainfall events, the concentration drops, and once it stops, the concentration of coarse particles rises due to resuspended road dust, construction activities, and wind-blown dust. During the monsoon months, from July to September, the daily concentration remains consistently below 30 $\mu g\ m^{-3}$. Similarly, studies suggested that non-combustion sources predominantly influence the PM_C concentration, which is higher during dry and windy conditions (Wong et al., 2021; Zhang et al., 2018a).

The 8-hour average O_3 concentration exceeds 46 days of the WHO limit (51 ppb for the 8-hour maximum limit) and 21 days of Nepal NAAQS (80 ppb for the 8-hour maximum limit). The results show that there is mostly a higher O_3 concentration in the pre-monsoon season, and the annual concentration of O_3 is 36.3 ± 14.3 ppb. The nighttime hourly average O_3 concentration drops to nearly zero in the winter and monsoon seasons. The variation of O_3 concentration is similar compared with the previous studies in Kathmandu Valley, but the daily concentration is higher than the previous measurements, such as Pulchowk, which is approximately 4 km away from the Khumaltar AQMS (Pudasainee et al., 2006) and Paknajol, approximately 8 km away from the Khumaltar AQMS (Mahata et al., 2018). The highest mean diurnal value was close to 90 ppb during the pre-monsoon season and about 10 ppb higher than the values reported in Mahata et al. (2018) for other sites in Kathmandu. This high value is in line with the general trend showing an

increase of O_3 concentrations in urban and background sites in South Asia (State of Global Air, 2024).

Furthermore, compared to urban sites in China (Xia et al., 2021; Li et al., 2022), the O_3 concentrations at the Khumaltar station are comparable to the highest concentrations 5% measured in China, revealing the issue of O_3 pollution in Kathmandu. Stratospheric intrusions can also impact altitude sites by elevating O_3 concentrations (Chen et al., 2024). The combination of altitude, where high concentrations of O_3 have already been recorded in the Himalayas (Kumar et al., 2010), and the presence of a large developing urban area could make Kathmandu one of the most exposed to high concentrations of O_3. Additionally, the high ozone concentration observed might be the result from stratosphere-troposphere exchange (STE). The interesting atmospheric phenomenon, tropopause folding and cut-off low events, can transport ozone from the stratosphere into the free troposphere (Cristofanelli et al., 2010; Kondratyev and Varotsos, 2002). The scientific evidence of such cases has been documented at high-altitude Himalayan sites Cristofanelli et al. (2010) that found the elevated surface ozone during pre-monsoon at the high altitude station (5079 m a.s.l.) in the central Himalayas was due to frequent STE-related enhancements of ozone showing intrusions from the stratosphere. Also, Kumar et al. (2010) observed high ozone levels at Nainital (India, 1958 m above mean sea level), with several episodes attributed to stratospheric intrusions. These findings suggest that, in addition to photochemical reactions, occasional stratosphere-troposphere exchange may partly explain the high ozone values observed at Kathmandu Valley, particularly during the pre-monsoon season when dynamical activity in the upper troposphere is stronger.

Both CO and NO_x concentrations show similar temporal variation during the study period, indicating a common emission source and similar atmospheric behavior for these pollutants within the Kathmandu Valley. The variation of daily average concentrations is shown in Figure 2. The annual CO concentration of 506 ± 172 ppb was recorded with a daily average ranging from 170 ppb to 1166 ppb. Similarly, the annual average NO_2 concentration of 10 ± 4 ppb was recorded, with significant daily variation ranging from 2 ppb to 25 ppb. The NO_2 concentration exceeds a WHO air quality guideline (8 ppb) in 223 days in the year. However, the concentration remains relatively stable throughout the year and consistently complies with the daily limits set by Nepal's NAAQS (25 ppb).

The annual concentration of SO_2 is 2.2 ± 1.1 ppb with a daily average

ranging from 1.3 ppb to 7.6 ppb. The measurement data reveal a unique time series of SO_2 concentrations at the site, and the concentrations increased from January to the end of May with values sometimes reaching 7.6 ppb. Beyond this period, the daily concentrations were constantly less than 2 ppb. The Figure 2e concentration of SO_2 suggests that concentrations are mainly influenced during this period by long-range transport without strong influences of local meteorology and emissions. Zhong et al. (2019) estimated that total SO_2 emissions in the Kathmandu Valley are approximately 308 tons per month, with brick kiln industries contributing over one-third of these emissions, and these industries typically operate during the period from mid-January to May.

3.2. Seasonal and diurnal variation

Figure 3 shows the seasonal variation of particulate matter and trace gases such as O_3, NO_x, CO, and SO_2. These pollutants exhibit a distinct seasonal and monthly variation, with a high peak in late winter and the pre-monsoon season. The monthly peaks of O_3 in April (58 $\pm$ 12 ppb monthly average), while the lowest monthly average occurs in August (19 $\pm$ 4 ppb), as shown in Figure 3a. Seasonally, the highest concentrations were observed during the pre-monsoon season (54 $\pm$ 5 ppb) and the lowest during the monsoon season (27 $\pm$ 13 ppb). The results indicate a similar behavior of air pollutants, including O_3, but the concentration levels are higher compared to previous studies conducted in the Kathmandu Valley (Mahata et al., 2018). This suggests that O_3 concentrations are increasing in the valley.

Similarly, CO, NO_x data (Figure 3b and Figure 3c) show that the highest concentration was found in winter and the pre-monsoon season, but the lowest was recorded in the monsoon. The monthly highest average concentration of NO_x (20 $\pm$ 5 ppb) was observed in January, and the lowest in September (5 $\pm$ 1 ppb). These findings highlight significant seasonal variation, with the highest pollution in winter (18 ppb) and the lowest in the monsoon season (5 ppb). The seasonal concentrations of CO were observed to be 713 ppb in winter, 572 ppb during the pre-monsoon period, 417 ppb in the post-monsoon, and 322 ppb during the monsoon. Usually, winter and pre-monsoon months comparatively exhibit higher levels of NO_x and CO due to increased emissions from biomass burning activities such as residential heating, garbage burning, and brick kilns, which are more prevalent during the dry months (Bhardwaj et al., 2018; Kiros et al., 2016). Furthermore, the valley's bowl-shaped topography, combined with meteorological factors such as weak winds, temperature

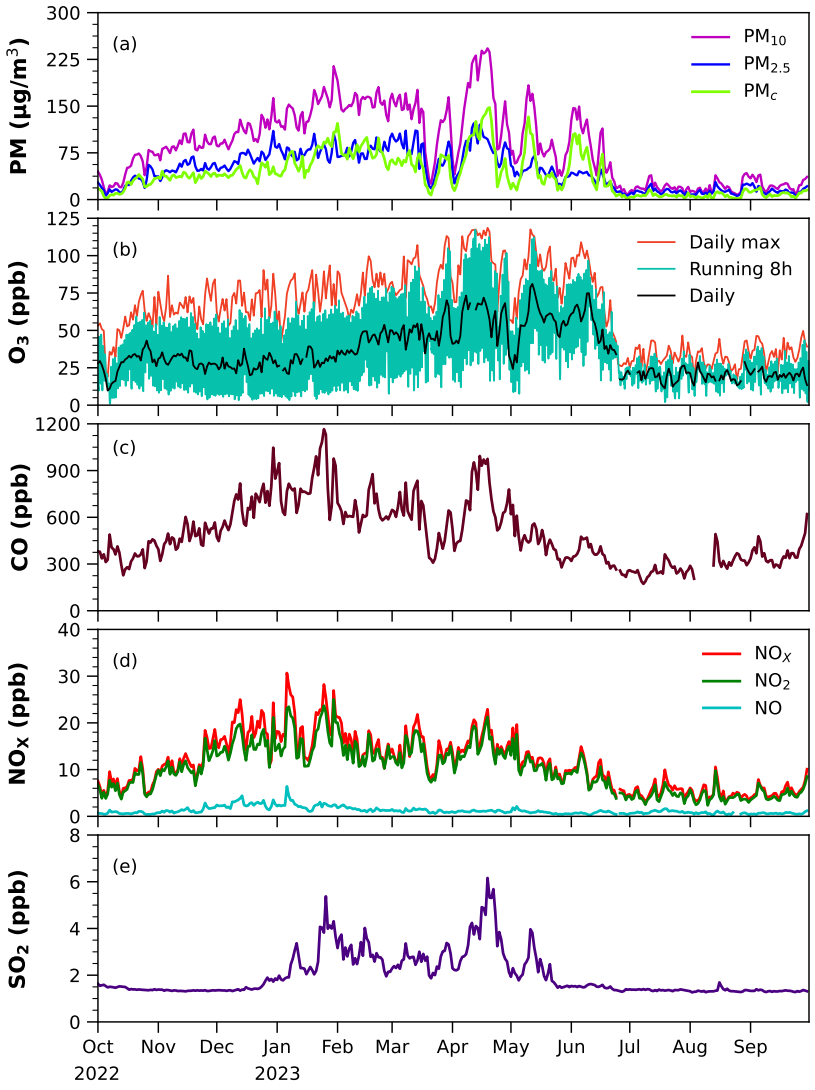

Figure 2: Temporal variation of air pollutant concentration from October 2022 to September 2023, including daily average concentrations for (a) PM_{10}, $PM_{2.5}$, PM_C, (b) O_3: daily maximum based on hourly data, 8-hour running average and daily average, and daily average concentrations for (c) CO, (d) NO_x, and (e) SO_2.

inversions, and reduced atmospheric mixing, results in poor dispersion of pollutants during winter, causing their accumulation near the surface (Panday and Prinn, 2009; Regmi et al., 2019). Conversely, the monsoon months bring heavy rain and increase the humidity, which supports wet deposition and the removal of air pollutants, resulting in the lowest concentrations (Gautam et al., 2023).

$PM_{2.5}$ (Figure 3h) shows a distinct seasonal variation, with concentrations peaking in winter, particularly in January and February, and during the pre-monsoon period, mainly in April. The lowest concentrations are observed during the monsoon season. Similarly, PM_{10} (Figure 3f) and PM_C (Figure 3g) are higher during the winter and pre-monsoon seasons. During winter, air pollutant concentrations in the Kathmandu Valley, particularly PM, increase due to enhanced emissions from biomass and waste burning as well as brick kiln operations (Islam et al., 2022). Moreover, PM concentration also depends on the boundary layer height and long-range transport, but it varies with season (Mues et al., 2017). Table 3 shows the seasonal comparison of our study with Aryal et al. (2009) study, carried out in Kathmandu almost two decades (17 years) ago. $PM_{2.5}$ concentrations have slightly decreased, but the previous study's measurement site was located in the highly urbanized residential area called Thamel (27^o $42'$ $21''$N; 85^o $19'$ $20''$E, Elevation 1314 m a.s.l.) approximately 8 km from the ICIMOD AQMS. Furthermore, measurements were conducted using low-volume air samplers based on the gravimetric method.

Table 3: Seasonal comparison of fine particulate matter concentrations (mean ± standard deviation) with previous measurements approximately 8 km away (Thamel) from ICIMOD AQMS.

Season	**Measurement in 2023 of $PM_{2.5}$ ($\mu g\ m^{-3}$)**	**Measurement in 2006 of $PM_{2.5}$ ($\mu g\ m^{-3}$)**
Post-Monsoon	38 ± 17	53 ± 22
Winter	75 ± 8	90 ± 24
Pre-Monsoon	66 ± 19	69 ± 37
Monsoon	18 ± 8	30 ± 12

The seasonal diurnal variation of the PM and trace gaseous pollutants at the site is shown in Figure 4. The diurnal variation of the O_3 is well defined with lower levels observed in the early morning and peaks occurring in the afternoon, particularly during the pre-monsoon. A higher daytime

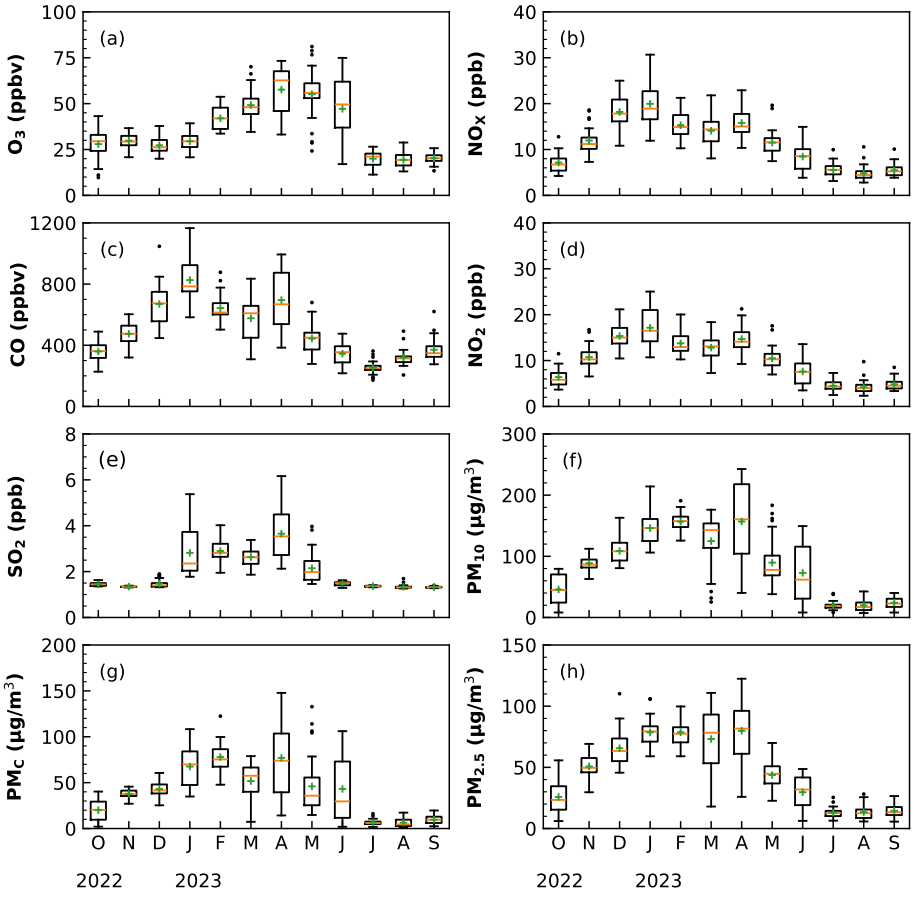

Figure 3: The monthly variations of (a) O_3, (b) NO_x, (c) CO, (d) NO_2, (e) SO_2, (f) PM_{10}, (g) PM_C, and (h) $PM_{2.5}$ in a year of measurement data from October 2022 to September 2023.

O_3 concentration is shown in the pre-monsoon season and is comparatively the lowest in the monsoon. The lowest concentrations during the monsoon season are likely due to increased cloud cover and rainfall, which can reduce photochemical reactions and enhance O_3 removal from the atmosphere (Lu et al., 2018). The CO, NO_x, PM_{10}, and $PM_{2.5}$ show perfect diurnal patterns with the morning and evening peaks for all seasons in the Figure 4. The concentration of pollution during the morning peak is generally higher than in the evening, primarily due to a lower boundary layer height in the morning, which restricts vertical mixing and limits pollutant dispersion. This, combined with the accumulation of pollutants emitted overnight from local sources, including vehicular emissions, leading to elevated pollution levels during the early hours of the day (Panday and Prinn, 2009). Unlike other pollutants, PM_C typically does not show distinct morning and evening peaks. Instead, its daily variation pattern closely resembles that of O_3 concentration. This is primarily due to differences in source characteristics, meteorological influences, and particle behavior. Coarse particles, having greater mass and aerodynamic diameter, tend to settle more rapidly through dry deposition, especially under stable atmospheric conditions (Wu et al., 2018). During the day, increased solar radiation, anthropogenic activity, and wind speed contribute to the redistribution of coarse particles rather than their accumulation (Barmpadimos et al., 2012).

The diurnal variation, particularly for NO_x, NO_2, and NO, shows a seasonal shift in peak times. During winter, the morning peak occurs around 9:00 AM, approximately one hour later than in other seasons (typically around 8:00 AM), likely due to delayed boundary layer development under stable morning conditions, consistent with earlier ceilometer-based observations in the Kathmandu Valley showing slower growth of the mixing layer height during winter (Mues et al., 2017). Similarly, the evening peak shifts to around 6:00 PM, one hour earlier than the usual 7:00 PM peak observed in warmer months. These diurnal profiles are commonly observed in urban areas and can be used to assess the evolution of traffic-related emissions by minimizing the influence of meteorological variability (Menut et al., 2012). NO_x emission sources in the Kathmandu Valley remain relatively constant throughout the year, primarily due to continuous road traffic activity, which dominates local emissions (Fukusaki et al., 2021). Diurnal patterns of SO_2 are evident during the winter and pre-monsoon seasons, whereas no such variation is observed in the monsoon and post-monsoon periods, when concentrations remain consistently below 2 ppb. A previous measurement con-

ducted about 4 km from the Khumaltar AQMS in 2001 similarly reported the absence of diurnal peaks even during February and March (Shresthal et al., 2002). The SO_2 levels observed during the pre-monsoon season at Khumaltar AQMS are comparable to those reported for the Kathmandu Valley by Kiros et al. (2016). This suggests that the sources of SO_2 in Kathmandu Valley are relatively stable and not significantly influenced by daily activities, and also influenced by meteorological conditions such as increased rainfall and humidity, which can enhance the removal of SO_2 from the atmosphere through wet deposition and its transformation to sulfate by non-linear chemistry (Ansari et al., 2025). However, the concentrations of trace gases such as NO_2, SO_2, and O_3 in the Kathmandu Valley are higher than those observed in a polluted European city (Tzanis et al., 2009).

3.3. Interspecies correlations

Interspecies correlation can be used to understand the source of pollutants, chemical formation, removal processes, and relations between atmospheric chemistry. Figure 5 presents a correlation plot of various species, showing correlation coefficients (r) and corresponding p-values for the entire dataset during the study period. The plot uses color-coded markers to distinguish the influence of temperature and humidity on these relationships. Figure 5a, O_3 and NO_x show an overall positive correlation ($r = 0.27$, $p = 0.00$). This relationship between species shows a minimum or even negative correlation at low air temperatures, which can be attributed to enhanced nighttime titration of O_3 by NO and reduced solar radiation. These conditions suppress photochemical O_3 production, resulting in a negative correlation between O_3 and NO_x during periods of weak solar radiation. In contrast, a positive correlation between O_3 and NO_x is observed at higher air temperatures during the daytime, typically associated with stronger solar radiation and increased photochemical activity. Similarly, a study shows the O_3 concentration reaches a minimum level during the cold season and nighttime due to NO titration and less solar radiation (Nguyen et al., 2024). $PM_{2.5}$ and O_3 concentrations tend to be positively correlated on average ($r = 0.51$, $p = 0.00$), especially during periods of high air temperatures. This positive relationship is most pronounced in the summer months, when higher temperatures and intense solar radiation promote the formation of O_3. In contrast, during colder conditions, particularly in winter and monsoon season, when the temperature is around 16 °C, the correlation between $PM_{2.5}$ and O_3 becomes lower or even negative. This occurrs in urban areas, where

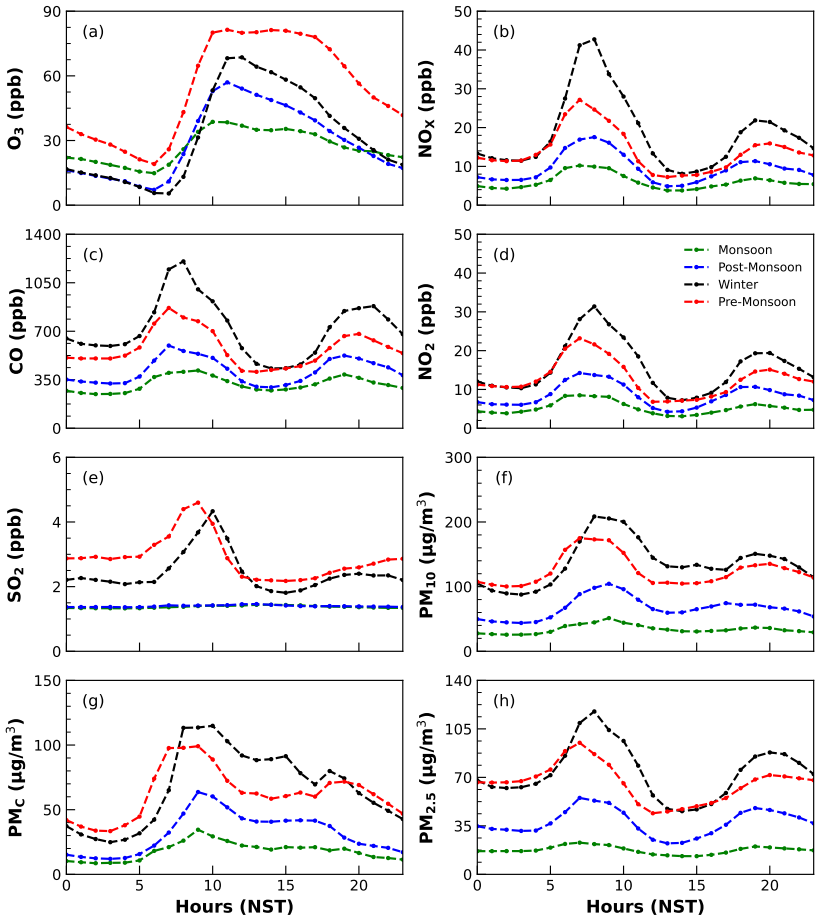

Figure 4: The Diurnal variations of (a) O_3, (b) NO_x, (c) CO, (d) NO_2, (e) SO_2, (f) PM_{10}, (g) PM_C, and (h) $PM_{2.5}$ in a year of measurement data from October 2022 to September 2023.

a study reveals that $PM_{2.5}$ and O_3 are negatively correlated in winter due to primary emissions and NO titration, but positively correlated in summer due to photochemical reactions (Nie et al., 2025).

Figure 5b shows a statistically significant moderate positive correlation (r = 0.58, p = 0.00)between SO_2 and NO_x, with their relationship being more pronounced under conditions of decreased relative humidity, as indicated by the color scale. This observation is consistent with studies demonstrating enhanced interactions between these pollutants even in humid conditions due to secondary air pollutant formation processes (Kazi et al., 2023). The scattering of the data at low humidity shows a complex interaction, probably influenced by varying emission sources and atmospheric dispersion processes. A recent study reported a significant correlation between SO_2 and NO_x ambient concentrations, as well as their emissions, often related to a common source such as fossil fuel combustion and industrial processes (Liu et al., 2022). Figure 5d shows a strong correlation between $PM_{2.5}$ and NO_x (r=0.82, p=0.00), indicating that $PM_{2.5}$ and NO_x are likely emitted from the same emission source in Kathmandu. It suggests that the high-temperature combustion sources, including vehicular emissions, significantly contribute to the fine particulate matter pollution level in Kathmandu Valley. A similar study by Varotsos et al. (2012) found a strong positive correlation between particulate matter and NO concentrations in urban areas during both peak and normal traffic periods. This suggests that traffic emissions are a major contributor to urban air pollution. Furthermore, secondary particulate matter formation is influenced by the chemical reaction rate of SO_2 and NO_x, which leads to increased sulfate and nitrate aerosol production under favorable atmospheric conditions such as high oxidant levels and humidity (Kong et al., 2020; Sun et al., 2013).

3.4. Relationship between coarse particles and meteorology

As shown in Figure 4, the diurnal evolution of the PM_C concentration shows a maximum during the day. PM_C is emitted by anthropogenic sources but can be largely influenced by resuspension processes, which depend on meteorological parameters. To examine the influence of meteorological factors on PM_{cf} and PM_C, a correlation analysis has been conducted between PM_{cf}, PM_C, and RH (Relative Humidity), Temperature, and wind speed (Figure 6). PM_{cf} and PM_C show a very strong negative correlation with RH (r = -0.80, p=0.00) and (r = -0.89, p=0.00), respectively, at Khumaltar station. The results show a maximum negative correlation (r = -0.92, p=0.00) during

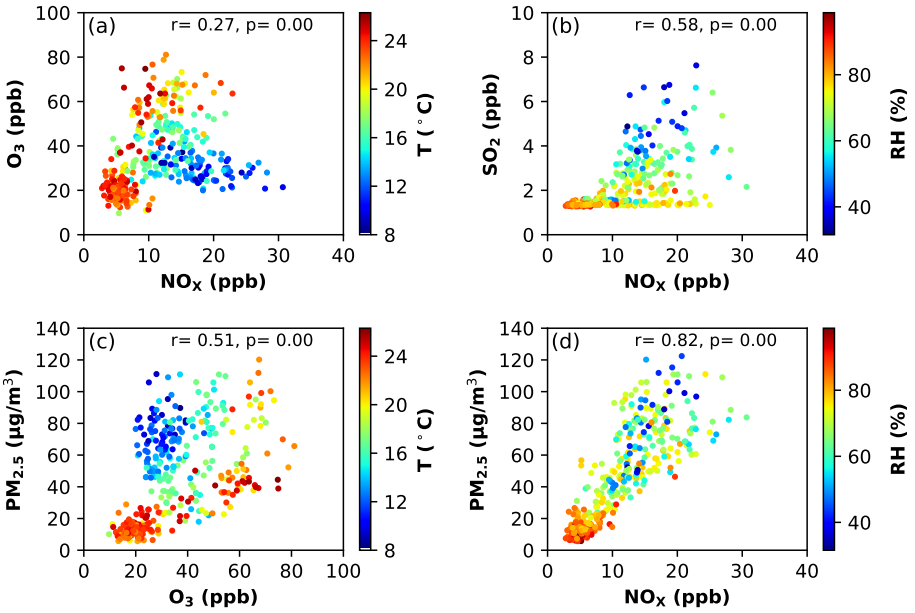

Figure 5: Interspecies relation scatter plots (a) NO_x - O_3 with color-coded air temperature, (b) NO_x - SO_2 with color-coded relative humidity, (c) O_3 - $PM_{2.5}$ with color-coded air temperature, (d) NO_x - $PM_{2.5}$ with color-coded relative humidity.

the monsoon season, with similar correlations observed in winter (r = -0.84, p=0.00), post-monsoon (r = -0.83, p=0.00), and pre-monsoon (r = -0.83, p=0.00) seasons. This suggests that higher relative humidity is statistically associated with lower PM_C concentrations, likely due to enhanced particle removal processes under humid conditions. Moreover, the strong negative correlation observed during the monsoon season reflects the strong influence of meteorological variability on particulate concentrations. Similar relationships have been reported by Islam et al. (2023) in Bangladesh, showing that higher relative humidity is often associated with reduced PM_C levels. This association can be attributed to precipitation-related washout and reduced resuspension of coarse particles, as well as the enhanced removal efficiency of larger particles under humid conditions (Liu et al., 2013). Similarly, PM concentrations in the Kathmandu Valley are notably lower during the monsoon and post-monsoon seasons, primarily due to enhanced wet deposition to the earth's surface through precipitation and scavenging processes. The strong negative correlation with RH aligns with findings by Hassan et al. (2020), who reported similar patterns in urban areas within arid regions.

The correlation analysis between PM_C and wind speed from the Khumaltar AQMS station revealed a statistically significant negative correlation (r=-0.21, p=0.00). Although higher wind speeds can sometimes promote the resuspension of surface particles, the observed negative correlation indicates that, in the Kathmandu Valley, strong winds more effectively enhance atmospheric mixing and dispersion, leading to reduced coarse particle concentrations. While in the dry season, wind-blown dust emissions typically occur when wind speeds exceed a threshold that depends on soil moisture. However, at Khumaltar, the dominant effect appears to be removal and dispersion rather than soil emission, likely due to the limited extent of exposed soil surfaces (Linda et al., 2025). In contrast, road traffic resuspension is primarily driven by vehicle-induced turbulence on dusty surfaces. Although mechanistic models of traffic-related PM resuspension are limited, existing studies attempt to simulate emissions based on precipitation and soil moisture conditions (de la Paz et al., 2015; Denby et al., 2013; Vautard et al., 2005; Thorpe et al., 2007). In Kathmandu, dry conditions, exacerbated by ongoing construction and poor road infrastructure, lead to significant dust accumulation on streets (Napit et al., 2020). Trace metals such as Cr and Ni have been detected in residential and traffic-affected areas, indicating contributions from both natural and anthropogenic sources (Sahu and Basti, 2021). Relative humidity serves as a useful proxy for soil moisture and precipitation,

both of which play a critical role in modulating resuspension processes.

Wind speed is a known driver of dust emissions from erodible surfaces, particularly in desert and agricultural regions (Vautard et al., 2005; Bessagnet et al., 2008). However, at the Khumaltar AQMS in Kathmandu, wind speed does not appear to be a reliable predictor of PM_C, which is more strongly influenced by local resuspension processes, likely driven by road traffic activity. Considering the wind speed measured at the Kathmandu airport meteorological station in (Figure 6e), which has more synoptic representativeness, a slight positive correlation (r = 0.29, p = 0.00) between the coarse fraction PM_{Cf} and the wind speed is observed, revealing a potential regional contribution of wind-blown dust. Regardless of the wind speed used, the correlation between the absolute value of PM_C and wind speed is poor, with two competing processes, wind speed enhances emission but also increases dispersion (Figures 6d and 6f).

The coarse fraction of particles emitted by resuspension accounts for approximately 75 % of PM_{10}, then the fine fraction represents one-third of the PM coarse fraction according to Amato et al. (2012). Therefore, our capacity to reconstruct the coarse fraction of PM from resuspension due to road traffic informs us about the contribution of resuspension to the $PM_{2.5}$ fraction, which could increase in the future with the renewal of the auto fleet (Wang et al., 2022). Moreover, assuming that 25 % of the resuspended particles are assigned to the fine fraction close to road traffic sites, in that case, this contribution is probably higher in urban background sites because the largest particles will be deposited by sedimentation (while the smallest ones will be less affected) during their transport far from their source.

3.5. Frequency analysis of regional transport

Many studies have demonstrated that air pollutants can be transported over long distances. For instance, research conducted in China has shown that pollutants can travel extremely long ranges, such as from Mongolia to Hangzhou, China (Zhang et al., 2018b). This long-range transport phenomenon underscores the transboundary nature of air pollution and its impact on regional air quality.

To better understand wind patterns and air mass transport over the Khumaltar AQMS, the HYSPLIT model was used to compute the air mass back trajectory. The 48-hour seasonal backward trajectories from the ICIMOD AQMS were computed for all four seasons, namely post-monsoon, winter,

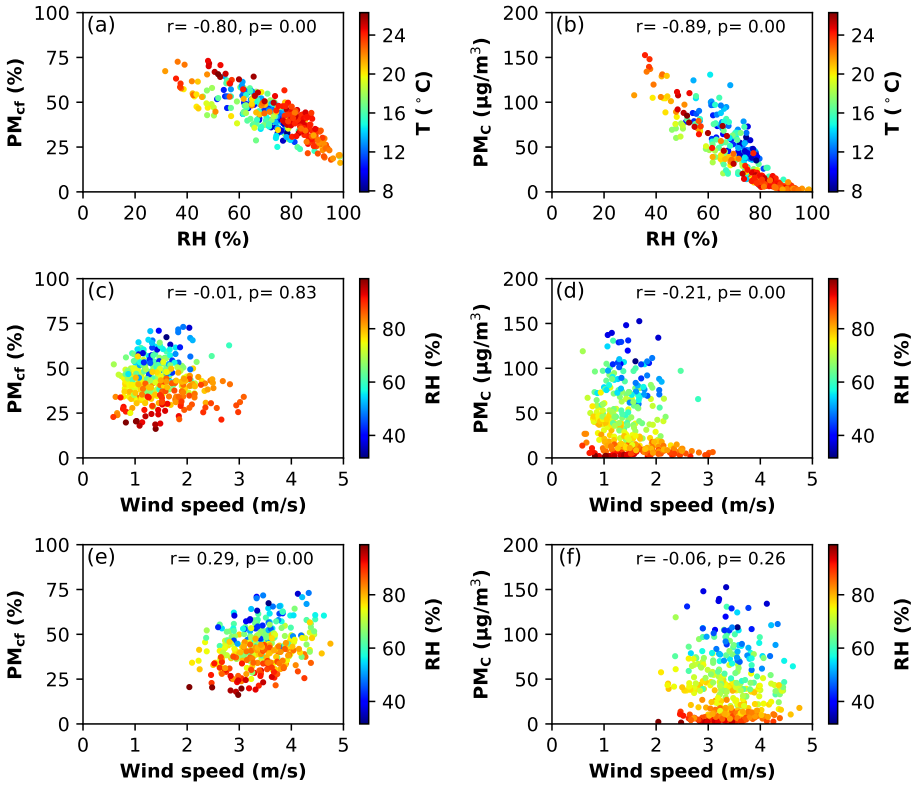

Figure 6: Scatter plots (a) PM_{cf} - RH and (b) PM_C - RH with color-coded air temperature, (c) PM_{cf} - wind speed and (d) PM_C - wind speed (ICIMOD station wind speed) and (e) PM_{cf} - wind speed and (f) PM_C - wind speed (Airport station wind speed) with color-coded relative humidity.

pre-monsoon, and monsoon. Figure 7 presents the seasonal average percentage of air masses arriving from various directions. The cluster analysis further illustrates the dominant transport pathways bringing air masses to the valley and the ICIMOD AQMS site from different directions: East (E), North (N), West (W), and South (S)in the four seasons. The dominant percentage of air mass comes from the southwest throughout the year. The trajectories initiated during the winter (65%) and pre-monsoon (78%) seasons are predominantly from the southwest, while the west was the dominant direction in the post-monsoon season (74%), and the southeast (66%) was the prevailing direction during the monsoon season. Certain trajectories exhibit long-range transport patterns, some of which extend over India and Bangladesh, indicating that pollutants can be transported over considerable distances. This directly implies that cross-border transportation also contributes to air quality in the Kathmandu Valley. The trajectories also show short-range transport patterns, showing the characteristics of slow-moving air masses. Most of the pollution episodes within this group are likely enriched by local emission sources and regional transport.

The findings are also similar to previous studies, such as a study conducted by Khanal et al. (2022) using the HYSPLIT backward trajectories to identify that the air mass originating from burning agricultural residues in North India (Punjab and Haryana) contributed to the source of air pollutants in the Kathmandu Valley. Similarly, a study shows that transported pollutants are a significant contributor to worsening air quality in the Kathmandu Valley, especially during the wildfire season. They also used HYSPLIT to identify the impact of forest fires in Kathmandu Valley (Kuikel et al., 2024). It implies that long-range pollutants transported, in addition to local sources, contributed to the deterioration of air quality within the valley.

This study is primarily based on a year-long measurement from Khumaltar AQMS, which provides detailed temporal insights but does not necessarily represent the full spatial variability of air pollution and its ground-level exposure across Kathmandu Valley. Therefore, the results are limited to generalize the community-level exposure without comprehensive community-based studies and surveys. Future research incorporating community-based sampling would enhance the representativeness of the findings.

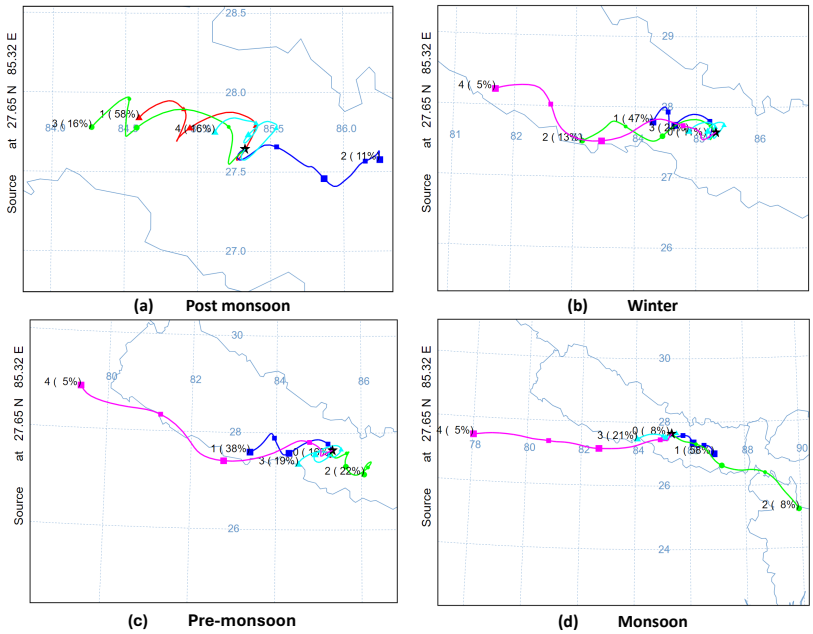

Figure 7: Seasonal cluster analysis of the 48-h air mass back trajectories starting at 100 m above ground level from the Khumaltar AQMS

.

4. Conclusions

This study provides a comprehensive year-long analysis of particulate matter and trace gases based on measurements taken at the Khumaltar AQMS. The findings reveal that $PM_{2.5}$ concentrations exceeded the WHO's annual guideline by more than nine times, emphasizing the serious air quality challenges faced by the Kathmandu Valley. Seasonally, concentrations of particulate matter and trace gases peak during the winter and pre-monsoon seasons, while they drop to their lowest concentration during the monsoon. Additionally, a strong correlation between $PM_{2.5}$ and NO_x indicates that fossil fuel combustion is the dominant source of fine particulate matter in the Valley. Meteorological factors, such as temperature and relative humidity, play a significant role in influencing the coarse fraction of PM concentration, with a strong negative correlation observed with RH. Furthermore, back-trajectory analysis shows that dominant westerly air mass flows occur during the winter and pre-monsoon seasons, suggesting that both local emissions and the regional pollutant transport contribute to air pollution in the Kathmandu Valley.

It will be important for the Kathmandu Valley to maintain such a station to capture a coherent trend of air pollution. More advanced equipments to analyse online the origin and source of particles would be an asset for the evaluation of the best strategies to improve air quality in the valley.

Acknowledgements

International Center for Integrated Mountain Development (ICIMOD) and its Regional Member Countries gratefully acknowledge the generous support of Austria, Norway, Sweden and Switzerland for core and programme funding, and the Adaptation Fund, Australia, Canada's International Development Research Centre, the European Union, Finland, Germany, Global Affairs Canada, Japan's Sasakawa Peace Foundation, the United Kingdom, and the World Bank for project funding.

References

Adhikary, B., Carmichael, G.R., Tang, Y., Leung, L.R., Qian, Y., Schauer, J.J., Stone, E.A., Ramanathan, V., Ramana, M.V., 2007. Characterization of the seasonal cycle of south Asian aerosols : A regional-scale modeling analysis 112, 1–22. doi:10.1029/2006JD008143.

Amato, F., Karanasiou, A., Moreno, T., Alastuey, A., Orza, J., Lumbreras, J., Borge, R., Boldo, E., Linares, C., Querol, X., 2012. Emission factors from road dust resuspension in a Mediterranean freeway. Atmospheric Environment 61, 580–587. URL: https://www.sciencedirect.com/science/article/pii/S1352231012007510, doi:https://doi.org/10.1016/j.atmosenv.2012.07.065.

Ansari, N., Kumari, P., Kumar, R., Kumar, P., Shamshad, A., Hossain, S., Sharma, A., Singh, Y., Kumari, M., Mishra, V.N., et al., 2025. Seasonal patterns of air pollution in Delhi: interplay between meteorological conditions and emission sources. Environmental Geochemistry and Health 47, 1–20.

Aryal, R.K., Lee, B.K., Karki, R., Gurung, A., Baral, B., Byeon, S.H., 2009. Dynamics of $PM_{2.5}$ concentrations in Kathmandu Valley, Nepal. Journal of Hazardous Materials 168, 732–738. doi:10.1016/j.jhazmat.2009.02.086.

Bagale, D., 2024. Temporal variability of seasonal and annual rainfall in Nepal. Journal of Nepal Hydrogeological Association 1, 57–66.

Bajgai, D.P., Shrestha, K.L., 2023. Evaluation of aircraft emission at Tribhuvan international airport and its contribution to air quality in Kathmandu, Nepal. Atmospheric Environment: X 17, 100204. URL: https://doi.org/10.1016/j.aeaoa.2023.100204, doi:10.1016/j.aeaoa.2023.100204.

Barmpadimos, I., Keller, J., Oderbolz, D., Hueglin, C., Prévôt, A., 2012. One decade of parallel fine ($PM_{2.5}$) and coarse (PM_{10}–$PM_{2.5}$) particulate matter measurements in Europe: trends and variability. Atmospheric Chemistry and Physics 12, 3189–3203.

Bender, J., Weigel, H.J., 2009. Changes in atmospheric chemistry and crop health. Sustainable Agriculture 2, 487–497. doi:10.1007/978-94-007-0394-0_22.

Bessagnet, B., Menut, L., Aymoz, G., Chepfer, H., Vautard, R., 2008. Modeling dust emissions and transport within Europe: The Ukraine March 2007 event. Journal of Geophysical Research: Atmospheres 113. URL: https://agupubs.onlinelibrary.wiley.com/doi/abs/10.1029/2007JD009541, doi:https://doi.org/10.1029/2007JD009541, arXiv:https://agupubs.onlinelibrary.wiley.c

Bhardwaj, P., Naja, M., Rupakheti, M., Lupascu, A., Mues, A., Panday, A.K., Kumar, R., Mahata, K.S., Lal, S., Chandola, H.C., Lawrence, M.G., 2018. Variations in surface ozone and carbon monoxide in the Kathmandu Valley and surrounding broader regions during SusKat-ABC field campaign: role of local and regional sources. Atmospheric Chemistry and Physics 18, 11949–11971. URL: https://acp.copernicus.org/articles/18/11949/2018/, doi:10.5194/acp-18-11949-2018.

Brunekreef, B., 2010. Air pollution and human health: From local to global issues. Procedia-Social and Behavioral Sciences 2, 6661–6669.

Castells-Quintana, D., Dienesch, E., Krause, M., 2021. Air pollution in an urban world: A global view on density, cities and emissions. Ecological Economics 189, 107153. URL: https://doi.org/10.1016/j.ecolecon.2021.107153, doi:10.1016/j.ecolecon.2021.107153.

Chen, Z., Liu, J., Qie, X., Cheng, X., Yang, M., Shu, L., Zang, Z., 2024. Stratospheric influence on surface ozone pollution in China. Nature Communications 15, 4064. URL: https://www.nature.com/articles/s41467-024-48406-x, doi:10.1038/s41467-024-48406-x.

Collins, W.J., Derwent, R.G., Johnson, C.E., Stevenson, D.S., 2002. The oxidation of organic compounds in the troposphere and their global warming potentials. Climatic Change 52, 453–479. doi:10.1023/A:1014221225434.

Colvile, R., Hutchinson, E.J., Mindell, J., Warren, R., 2001. The transport sector as a source of air pollution. Atmospheric environment 35, 1537–1565.

Cristofanelli, P., Bracci, A., Sprenger, M., Marinoni, A., Bonafè, U., Calzolari, F., Duchi, R., Laj, P., Pichon, J.M., Roccato, F., et al., 2010. Tropospheric ozone variations at the Nepal Climate Observatory-Pyramid (Himalayas, 5079 m asl) and influence of deep stratospheric intrusion events. Atmospheric Chemistry and Physics 10, 6537–6549.

Crutzen, P., 1973. A discussion of the chemistry of some minor constituents in the stratosphere and troposphere. Pure and Applied Geophysics PAGEOPH 106-108, 1385–1399. doi:10.1007/BF00881092.

Cui, L., Song, X., Zhong, G., 2021. Comparative analysis of three methods for HYSPLIT atmospheric trajectories clustering. Atmosphere 12, 698.

Das, B., Bhave, P.V., Puppala, S.P., Adhikari, S., Sainju, S., Mool, E., Byanju, R.M., 2022. Emission factors and emission inventory of diesel vehicles in Nepal. Science of the Total Environment 812, 152539. URL: https://doi.org/10.1016/j.scitotenv.2021.152539, doi:10.1016/j.scitotenv.2021.152539.

Das, B., Bhave, P.V., Sapkota, A., Byanju, R.M., 2018. Estimating emissions from open burning of municipal solid waste in municipalities of Nepal. Waste Management 79, 481–490. URL: https://www.sciencedirect.com/science/article/pii/S0956053X18304963, doi:https://doi.org/10.1016/j.wasman.2018.08.013.

Denby, B., Sundvor, I., Johansson, C., Pirjola, L., Ketzel, M., Norman, M., Kupiainen, K., Gustafsson, M., Blomqvist, G., Kauhaniemi, M., Omstedt, G., 2013. A coupled road dust and surface moisture model to predict non-exhaust road traffic induced particle emissions (NORTRIP). Part 2: Surface moisture and salt impact modelling. Atmospheric Environment 81, 485–503. URL: https://www.sciencedirect.com/science/article/pii/S1352231013006912, doi:https://doi.org/10.1016/j.atmosenv.2013.09.003.

Dentener, F., Stevenson, D., Cofala, J., Mechler, R., Amann, M., Bergamaschi, P., Raes, F., Derwent, R., 2005. The impact of air pollutant and methane emission controls on tropospheric ozone and radiative forcing: CTM calculations for the period 1990-2030. Atmospheric Chemistry and Physics 5, 1731–1755. doi:10.5194/acp-5-1731-2005.

Dhital, N.B., 2024. Comparing the characteristics of ambient fine particle pollution episodes across South Asian cities. Environmental Challenges 15, 100912. URL: https://doi.org/10.1016/j.envc.2024.100912, doi:10.1016/j.envc.2024.100912.

Faiz, A., Bahadur Ale, B., Nagarkoti, R.K., 2006. The role of inspection and maintenance in controlling vehicular emissions in Kathmandu valley, Nepal. Atmospheric Environment 40, 5967–5975. doi:10.1016/j.atmosenv.2005.11.064.

Fukusaki, Y., Umehara, M., Kousa, Y., Inomata, Y., Nakai, S., 2021. Investigation of Air Pollutants Related to the Vehicular Exhaust Emissions in the Kathmandu Valley, Nepal. Atmosphere 12, 1322.

Gautam, P., Blaha, U., Appel, E., 2005. Magnetic susceptibility of dust-loaded leaves as a proxy of traffic-related heavy metal pollution in Kathmandu city, Nepal. Atmospheric Environment 39, 2201–2211. URL: https://www.sciencedirect.com/science/article/pii/S135223100500052X, doi:https://doi.org/10.1016/j.atmosenv.2005.01.006.

Gautam, S., Silwal, A., Baral, B., Subedi, S., Lamichhane, N., Chapagain, N., Adhikari, B., 2023. Influence of the rainfall and temperature oscillation on air quality in Kathmandu valley: The wavelet analysis. Environmental Engineering Research 28.

González, C., Gómez, C., Rojas, N., Acevedo, H., Aristizábal, B., 2017. Relative impact of on-road vehicular and point-source industrial emissions of air pollutants in a medium-sized Andean city. Atmospheric environment 152, 279–289.

Grimm, H., Eatough, D.J., 2009. Aerosol measurement: the use of optical light scattering for the determination of particulate size distribution, and particulate mass, including the semi-volatile fraction. Journal of the Air & Waste Management Association 59, 101–107.

Hassan, H., Saraga, D., Kumar, P., Kakosimos, K.E., 2020. Vehicle-induced fugitive particulate matter emissions in a city of arid desert climate. Atmospheric Environment 229, 117450. URL: https://www.sciencedirect.com/science/article/pii/S1352231020301874, doi:https://doi.org/10.1016/j.atmosenv.2020.117450.

Huszar, P., Karlickỳ, J., Bartík, L., Liaskoni, M., Prieto Perez, A.P., Šindelářová, K., 2022. Impact of urbanization on gas-phase pollutant concentrations: a regional-scale, model-based analysis of the contributing factors. Atmospheric Chemistry and Physics 22, 12647–12674.

Islam, M.R., Li, T., Mahata, K., Khanal, N., Werden, B., Giordano, M.R., Praveen Puppala, S., Dhital, N.B., Gurung, A., Saikawa, E., et al., 2022. Wintertime air quality across the Kathmandu valley, Nepal: concentration,

composition, and sources of fine and coarse particulate matter. ACS Earth and space chemistry 6, 2955–2971.

Islam, N., Toha, T.R., Islam, M.M., Ahmed, T., et al., 2023. Spatio-temporal variation of meteorological influence on PM2. 5 and PM_{10} over major urban cities of Bangladesh. Aerosol and Air Quality Research 23, 220082.

Karki, R., Hasson, S.u., Schickhoff, U., Scholten, T., Böhner, J., 2017. Rising precipitation extremes across Nepal. Climate 5, 4.

Karki, R., Talchabhadel, R., Aalto, J., Baidya, S.K., 2016. New climatic classification of Nepal. Theoretical and applied climatology 125, 799–808.

Kazi, Z., Filip, S., Kazi, L., 2023. Predicting $PM_{2.5}$, PM_{10}, SO_2, NO_2, NO and CO air pollutant values with linear regression in R language. Applied Sciences 13, 3617.

Khanal, P., Gurung, A., Chand, P.B., 2017. Road expansion and urban highways: consequences outweigh benefits in Kathmandu. HIMALAYA, the Journal of the Association for Nepal and Himalayan Studies 37, 15.

Khanal, S., Pokhrel, R.P., Pokharel, B., Becker, S., Giri, B., Adhikari, L., LaPlante, M.D., 2022. An episode of transboundary air pollution in the central Himalayas during agricultural residue burning season in North India. Atmospheric Pollution Research 13, 101270.

Kiros, F., Shakya, K.M., Rupakheti, M., Regmi, R.P., Maharjan, R., Byanju, R.M., Naja, M., Mahata, K., Kathayat, B., Peltier, R.E., 2016. Variability of anthropogenic gases: Nitrogen oxides, sulfur dioxide, ozone and ammonia in Kathmandu Valley, Nepal. Aerosol and Air Quality Research 16, 3088–3101.

Kondratyev, K.Y., Varotsos, C., 2002. Remote sensing and global tropospheric ozone observed dynamics. International Journal of Remote Sensing 23, 159–178.

Kong, L., Feng, M., Liu, Y., Zhang, Y., Zhang, C., Li, C., Qu, Y., An, J., Liu, X., Tan, Q., et al., 2020. Elucidating the pollution characteristics of nitrate, sulfate and ammonium in $PM_{2.5}$ in Chengdu, southwest China based on long-term observations. Atmospheric Chemistry and Physics Discussions 2020, 1–38.

Kuikel, S., Pokharel, B., Bhattarai, N., 2024. The effect of wildfires on air quality in Kathmandu, Nepal. Environmental Advances 15, 100493.

Kumar, R., Naja, M., Venkataramani, S., Wild, O., 2010. Variations in surface ozone at Nainital: A high-altitude site in the central Himalayas. Journal of Geophysical Research: Atmospheres 115. URL: https://agupubs.onlinelibrary.wiley.com/doi/abs/10.1029/2009JD013715, doi:https://doi.org/10.1029/2009JD013715.

Li, L., Liu, N., Shen, L., Zhao, Z., Wang, H., Wang, Y., Li, X., Ma, Y., 2022. Ozone concentration at various heights near the surface layer in Shenyang, Northeast China. Frontiers in Environmental Science 10. URL: https://www.frontiersin.org/journals/environmental-science/articles/10.3389/fenv doi:10.3389/fenvs.2022.1011508.

Liao, T., Wang, S., Ai, J., Gui, K., Duan, B., Zhao, Q., Zhang, X., Jiang, W., Sun, Y., 2017. Heavy pollution episodes, transport pathways and potential sources of $PM_{2.5}$ during the winter of 2013 in Chengdu (China). Science of the Total Environment 584-585, 1056–1065. URL: http://dx.doi.org/10.1016/j.scitotenv.2017.01.160, doi:10.1016/j.scitotenv.2017.01.160.

Linda, J., Hasečić, A., Pospíšil, J., Kudela, L., Brzezina, J., 2025. Impact of wind-induced resuspension on urban air quality: a cfd study with air quality data comparison. npj Climate and Atmospheric Science 8, 74.

Liu, T., Li, T.T., Zhang, Y.H., Xu, Y.J., Lao, X.Q., Rutherford, S., Chu, C., Luo, Y., Zhu, Q., Xu, X.J., Xie, H.Y., Liu, Z.R., Ma, W.J., 2013. The short-term effect of ambient ozone on mortality is modified by temperature in Guangzhou, China. Atmospheric Environment 76, 59–67. URL: http://dx.doi.org/10.1016/j.atmosenv.2012.07.011, doi:10.1016/j.atmosenv.2012.07.011.

Liu, X., Ran, L., Lin, W., Xu, X., Ma, Z., Dong, F., He, D., Zhou, L., Shi, Q., Wang, Y., 2022. Measurement report: Variations in surface SO_2 and NOx mixing ratios from 2004 to 2016 at a background site in the North China Plain. Atmospheric Chemistry and Physics Discussions 2022, 1–23.

Lu, X., Zhang, L., Liu, X., Gao, M., Zhao, Y., Shao, J., 2018. Lower tropospheric ozone over India and its linkage to the South Asian monsoon. Atmospheric Chemistry and Physics 18, 3101–3118.

Maciejewska, K., 2020. Short-term impact of $PM_{2.5}$, PM_{10}, and PMc on mortality and morbidity in the agglomeration of Warsaw, Poland. Air Quality, Atmosphere & Health 13, 659–672.

Maharjan, M., Yoneda, M., Talchabhadel, R., Thapa, B.R., Aryal, A., 2023. Use of indices on daily timescales to study changes in extreme precipitation across Nepal over 40 years (1976–2015). Earth and Space Science 10, e2020EA001509.

Mahata, K.S., Rupakheti, M., Kumar Panday, A., Bhardwaj, P., Naja, M., Singh, A., Mues, A., Cristofanelli, P., Pudasainee, D., Bonasoni, P., Lawrence, M.G., 2018. Observation and analysis of spatiotemporal characteristics of surface ozone and carbon monoxide at multiple sites in the Kathmandu Valley, Nepal. Atmospheric Chemistry and Physics 18, 14113–14132. doi:10.5194/acp-18-14113-2018.

Matthaios, V.N., Lawrence, J., Martins, M.A.G., Ferguson, S.T., Wolfson, J.M., Harrison, R.M., Koutrakis, P., 2022. Science of the Total Environment. Science of the Total Environment 835, 155368. URL: https://doi.org/10.1016/j.scitotenv.2022.155368, doi:10.1016/j.scitotenv.2022.155368.

Menut, L., Goussebaile, A., Bessagnet, B., Khvorostiyanov, D., Ung, A., 2012. Impact of realistic hourly emissions profiles on air pollutants concentrations modelled with CHIMERE. Atmospheric Environment 49, 233–244. URL: https://www.sciencedirect.com/science/article/pii/S1352231011012441, doi:https://doi.org/10.1016/j.atmosenv.2011.11.057.

Mues, A., Rupakheti, M., Münkel, C., Lauer, A., Bozem, H., Hoor, P., Butler, T., Lawrence, M.G., 2017. Investigation of the mixing layer height derived from ceilometer measurements in the Kathmandu Valley and implications for local air quality. Atmospheric Chemistry and Physics 17, 8157–8176. doi:10.5194/acp-17-8157-2017.

Mukherjee, A., Agrawal, M., 2017. World air particulate matter: sources, distribution and health effects. Environmental chemistry letters 15, 283–309.

NAAQS, 2012. Nepal National Ambient Air Quality Standard 2012. URL: https://nepalindata.com/resource/National-Ambient-Air-Quality-Standard-2012/.

Napit, A., Shakya, S., Shrestha, M., Shakya, R.K., Shrestha, P.K., Pradhananga, A.R., Ghimire, N.G., Pant, D.R., Shakya, P.R., 2020. Pollution Characteristics and Human Health Risks to Heavy Metals Exposure in Street Dust of Kathmandu, Nepal. Advanced Journal of Chemistry-Section A 3. URL: https://doi.org/10.22034/ajca.2020.106231, doi:10.22034/ajca.2020.106231.

Nguyen, D.H., Liao, C.H., Bui, X.T., Wang, L.C., Yuan, C.S., Lin, C., 2024. Deseasonalized trend of ground-level ozone and its precursors in an industrial city Kaohsiung, Taiwan. Environmental Pollution 351, 124036.

Nie, Y., Yan, Y., Ji, Y., Gao, R., Ren, Y., Bi, F., Shang, F., Li, J., Chu, W., Li, H., 2025. Assessing the $PM_{2.5}$–O_3 Correlation and Unraveling Their Drivers in Urban Environment: Insights from the Bohai Bay Region, China. Atmosphere 16, 512.

Nuvolone, D., Petri, D., Voller, F., 2018. The effects of ozone on human health. Environmental Science and Pollution Research 25, 8074–8088. doi:10.1007/s11356-017-9239-3.

Panday, A.K., Prinn, R.G., 2009. Diurnal cycle of air pollution in the kathmandu valley, nepal: Observations. Journal of Geophysical Research Atmospheres 114, 1–19. doi:10.1029/2008JD009777.

de la Paz, D., Borge, R., Vedrenne, M., Lumbreras, J., Amato, F., Karanasiou, A., Boldo, E., Moreno, T., 2015. Implementation of road dust resuspension in air quality simulations of particulate matter in Madrid (Spain). Frontiers in Environmental Science 3. URL: https://www.frontiersin.org/journals/environmental-science/articles/10.3389/fenv doi:10.3389/fenvs.2015.00072.

Phairuang, W., Suwattiga, P., Hongtieab, S., Inerb, M., Furuuchi, M., Hata, M., 2021. Characteristics, sources, and health risks of ambient nanoparticles (PM0.1) bound metal in Bangkok, Thailand. Atmospheric Environment: X 12, 100141.

Pudasainee, D., Sapkota, B., Shrestha, M.L., Kaga, A., Kondo, A., Inoue, Y., 2006. Ground level ozone concentrations and its association with NOx and meteorological parameters in Kathmandu valley, Nepal. Atmospheric Environment 40, 8081–8087. doi:10.1016/j.atmosenv.2006.07.011.

Qin, Y., Kim, E., Hopke, P.K., 2006. The concentrations and sources of $PM_{2.5}$ in metropolitan New York City. Atmospheric Environment 40, 312–332. doi:10.1016/j.atmosenv.2006.02.025.

Regmi, R.P., Kitada, T., Maharjan, S., Shrestha, S., Shrestha, S., Regmi, G., 2019. Wintertime boundary layer evolution and air pollution potential over the Kathmandu Valley, Nepal. Journal of Geophysical Research: Atmospheres 124, 4299–4325.

Sadavarte, P., Rupakheti, M., Bhave, P., Shakya, K., Lawrence, M., 2019. Nepal emission inventory–Part I: Technologies and combustion sources (NEEMI-Tech) for 2001–2016. Atmospheric Chemistry and Physics 19, 12953–12973.

Sahu, C., Basti, S., 2021. Trace metal pollution in the environment: a review. International Journal of Environmental Science and Technology 18, 211–224.

Shresthal, M.L., Kagal, A., Kondol, A., Inouel, Y., Sapkota, B., 2002. Diurnal variation of air pollution concentration during winter in Kathmandu valley .

Singh, V., Biswal, A., Kesarkar, A.P., Mor, S., Ravindra, K., 2020. Science of the Total Environment High resolution vehicular PM_{10} emissions over megacity Delhi : Relative contributions of exhaust and non-exhaust sources. Science of the Total Environment 699, 134273. URL: https://doi.org/10.1016/j.scitotenv.2019.134273, doi:10.1016/j.scitotenv.2019.134273.

State of Global Air, 2024. Soga-2024-Report_0.Pdf. URL: https://www.stateofglobalair.org/sites/default/files/documents/2024-06/soga-2024

Stein, A.F., Draxler, R.R., Rolph, G.D., Stunder, B.J., Cohen, M.D., Ngan, F., 2015. NOAA's HYSPLIT atmospheric transport and dispersion modeling system. Bulletin of the American Meteorological Society 96, 2059–2077.

Sun, G., Yao, L., Jiao, L., Shi, Y., Zhang, Q., Tao, M., Shan, G., He, Y., 2013. Characterizing PM2. 5 pollution of a subtropical metropolitan area in China. Atmospheric and Climate Sciences 3, 100–110.

Sun, Y., Wang, L., Wang, Y., Zhang, D., Quan, L., Jinyuan, X., 2010. In situ measurements of NO, NO_2, NOy, and O_3 in Dinghushan (112°E, 23°N), China during autumn 2008. Atmospheric Environment 44, 2079–2088. URL: http://dx.doi.org/10.1016/j.atmosenv.2010.03.007, doi:10.1016/j.atmosenv.2010.03.007.

Thorpe, A.J., Harrison, R.M., Boulter, P.G., McCrae, I.S., 2007. Estimation of particle resuspension source strength on a major London Road. Atmospheric Environment 41, 8007–8020. URL: https://www.sciencedirect.com/science/article/pii/S1352231007006139, doi:https://doi.org/10.1016/j.atmosenv.2007.07.006.

Tzanis, C., Varotsos, C., Christodoulakis, J., Tidblad, J., Ferm, M., Ionescu, A., Lefevre, R.A., Theodorakopoulou, K., Kreislova, K., 2011. On the corrosion and soiling effects on materials by air pollution in athens, greece. Atmospheric Chemistry and Physics 11, 12039–12048.

Tzanis, C., Varotsos, C., Ferm, M., Christodoulakis, J., Assimakopoulos, M., Efthymiou, C., 2009. Nitric acid and particulate matter measurements at athens, greece, in connection with corrosion studies. Atmospheric Chemistry and Physics 9, 8309–8316.

Varotsos, C., Ondov, J., Tzanis, C., Öztürk, F., Nelson, M., Ke, H., Christodoulakis, J., 2012. An observational study of the atmospheric ultrafine particle dynamics. Atmospheric Environment 59, 312–319.

Vautard, R., Bessagnet, B., Chin, M., Menut, L., 2005. On the contribution of natural Aeolian sources to particulate matter concentrations in Europe : Testing hypotheses with a modelling approach 39, 3291–3303. doi:10.1016/j.atmosenv.2005.01.051.

Wang, M., Duan, Y., Zhang, Z., Huo, J., Huang, Y., Fu, Q., Wang, T., Cao, J., cheng Lee, S., 2022. Increased contribution to $PM_{2.5}$ from traffic-influenced road dust in Shanghai over recent years and predictable future. Environmental Pollution 313, 120119. URL: https://www.sciencedirect.com/science/article/pii/S0269749122013331, doi:https://doi.org/10.1016/j.envpol.2022.120119.

Wang, Q., Kwan, M.P., Zhou, K., Fan, J., Wang, Y., Zhan, D., 2019. The impacts of urbanization on fine particulate matter ($PM_{2.5}$) concentrations:

Empirical evidence from 135 countries worldwide. Environmental pollution 247, 989–998.

Wester, P., Mishra, A., Mukherji, A., Shrestha, A.B., 2019. The Hindu Kush Himalaya Assessment: Mountains, Climate Change, Sustainability and People. Springer International Publishing. URL: http://dx.doi.org/10.1007/978-3-319-92288-1_10, doi:10.1007/978-3-319-92288-1.

WHO, 2021. WHO global air quality guidelines. Particulate matter ($PM_{2.5}$ and PM_{10}), ozone, nitrogen dioxide, sulfur dioxide and carbon monoxide. , 1–360.

Wong, Y.K., Liu, K.M., Yeung, C., Leung, K.K., Yu, J.Z., 2021. Measurement report: Characterization and source apportionment of coarse particulate matter in Hong Kong: insights into the constituents of unidentified mass and source origins in a coastal city in southern China. Atmospheric Chemistry and Physics Discussions 2021, 1–23.

World Bank, 2025. Towards Clean Air in Nepal: Benefits, Pollution Sources, and Solutions. Technical Report. World Bank. Washington, DC. URL: https://hdl.handle.net/10986/43303. license: CC BY-NC 3.0 IGO.

Wu, Y., Liu, J., Zhai, J., Cong, L., Wang, Y., Ma, W., Zhang, Z., Li, C., 2018. Comparison of dry and wet deposition of particulate matter in near-surface waters during summer. PloS one 13, e0199241.

Xia, N., Du, E., Guo, Z., de Vries, W., 2021. The diurnal cycle of summer tropospheric ozone concentrations across Chinese cities: Spatial patterns and main drivers. Environmental Pollution 286, 117547. URL: https://www.sciencedirect.com/science/article/pii/S0269749121011295, doi:https://doi.org/10.1016/j.envpol.2021.117547.

Yu, J., Cai, M., Zhou, Y., Ou, J., 2025. An Improved Water Vapor Trajectory Clustering Method and Its Application Analysis. Open Journal of Applied Sciences 15, 1033–1049.

Zhang, B., Jiao, L., Xu, G., Zhao, S., Tang, X., Zhou, Y., Gong, C., 2018a. Influences of wind and precipitation on different-sized particulate matter concentrations ($PM_{2.5}$, PM_{10}, $PM_{2.5--10}$). Meteorology and Atmospheric Physics 130, 383–392.

Zhang, G., Xu, H., Qi, B., Du, R., Gui, K., Wang, H., Jiang, W., Liang, L., Xu, W., 2018b. Characterization of atmospheric trace gases and particulate matter in Hangzhou, China. Atmospheric Chemistry and Physics 18, 1705–1728.

Zhong, M., Saikawa, E., Avramov, A., Chen, C., Sun, B., Ye, W., Keene, W.C., Yokelson, R.J., Jayarathne, T., Stone, E.A., Rupakheti, M., Panday, A.K., 2019. Nepal Ambient Monitoring and Source Testing Experiment (NAMaSTE): Emissions of particulate matter and sulfur dioxide from vehicles and brick kilns and their impacts on air quality in the Kathmandu Valley, Nepal. Atmospheric Chemistry and Physics 19, 8209–8228. doi:10.5194/acp-19-8209-2019.